# Probing the goldstino excitation through tunneling transport in a Bose-Fermi mixture with explicitly broken supersymmetry

Tingyu Zhang [1,2,*] Yixin Guo [1,2,†] Hiroyuki Tajima [1,‡] and Haozhao Liang [1,2,§]
[1]*Department of Physics, School of Science, The University of Tokyo, Tokyo 113-0033, Japan*
[2]*Interdisciplinary Theoretical and Mathematical Sciences Program, RIKEN, Wako 351-0198, Japan*

(Received 15 May 2024; revised 31 July 2024; accepted 7 August 2024; published 22 August 2024)

We theoretically investigate the tunneling transport in a repulsively interacting ultracold Bose-Fermi mixture. A two-terminal model is applied to such a mixture, and the supersymmetry-like tunneling current through the junction can be induced by the bias of the fermion chemical potential between two reservoirs. The goldstino, which is the Nambu-Goldstone fermionic mode associated with the spontaneous sypersymmetry breaking and appears as a gapped mode in the presence of the explicit supersymmetry breaking in existing Bose-Fermi mixtures, is found to contribute to the tunneling transport as a supercharge exchanging process. Our study provides a potential way to detect the goldstino transport in cold atom experiments.

DOI: 10.1103/PhysRevB.110.064512

## I. INTRODUCTION

Quantum transport phenomena serve as a crucial avenue for understanding complex quantum many-body systems, with extensive exploration in condensed matter physics, atomic physics, and nuclear physics. The unique characteristics of cold atomic systems, such as controllable interaction strength, variable species number, and densities, make them an ideal platform for investigating phenomena challenging to realize in solid-state systems. The Feshbach resonances for adjusting interparticle scattering length enable us to explore strongly interacting regimes [1]. The density manipulation of atomic species allows for the direct induction and measurement of quantum transport [2–4]. Leveraging the cleanness, high controllability, and advanced experimental techniques of cold atomic systems, researchers have observed and investigated diverse transport phenomena, including bulk spin transport [5–7], multiple Andreev reflections [8], and the Josephson effect [9–11].

Recently, an ultracold Bose-Fermi mixture [12–16] opened a novel path to a wide range of applications for investigating quantum many-body systems [17–21], including the possible realization of analog quantum simulations to achieve supersymmetry [22–28], dense hadron-quark matter [29–32], and neutron-rich nuclei [33–36]. Certain mixtures with a small mass imbalance are realized in experiments by using different isotopes, such as $^{6}$Li - $^{7}$Li [13,14,37], $^{39}$K - $^{40}$K [38], $^{40}$K - $^{41}$K [15], $^{84}$Sr - $^{87}$Sr [39], $^{161}$Dy - $^{162}$Dy [40], and $^{173}$Yb - $^{174}$Yb [41,42]. In such systems, the fermionic Nambu-Goldstone mode, which is called the goldstino [22,43–45], is generated when the supersymmetry, namely, the Fermi-Bose exchange symmetry, is broken. While the existence of the bosonic Nambu-Goldstone mode [46,47] has been confirmed experimentally in a cold atomic system [48], the existence of the goldstino has still been elusive. Such a situation is not limited to ultracold atomic physics, and it is still difficult to confirm the goldstino in nature. In this regard, it is an exciting challenge to detect the possible appearance of the goldstino in atomic systems.

A hint to find the consequence of the goldstino is that the goldstino can be regarded as an analog of the magnon mode, which is a collective excitation of spin structures in a ferromagnetic phase [49] and is also a type of Nambu-Goldstone boson. In repulsively interacting Fermi gases at low temperatures, magnons have been proposed to play a crucial role in spin transport, with its enhanced signal as the interaction strength increases [50,51]. While the magnon mode arises from the spin-flip process [52], involving the interchange of spin-up and spin-down particles, the goldstino corresponds to the interchange of bosonic and fermionic atoms. Accordingly, it raises the intriguing question of whether the goldstino contributes to transport in such mixtures and whether it can be identified through the measurement of tunneling current feasible in an ultracold atomic system. We note that even in the presence of the explicit supersymmetry breaking in a Bose-Fermi mixture (e.g., the imbalance of masses and chemical potentials between fermions and bosons), one can expect the goldstino excitation, but with the nonzero energy gap [28].

In this study, we propose a two-terminal model comprising ultracold Bose-Fermi mixtures, allowing for the tuning of species density to induce tunneling processes driven by a chemical potential bias between two reservoirs (see Fig. 1). The bosons predominantly exist in the Bose-Einstein condensate (BEC) phase with zero momentum below the BEC critical temperature, while the fermions form a fully filled Fermi sea. Assuming the fermions are polarized with only one remaining degree of freedom (i.e., a single hyperfine state), we consider the boson-fermion and boson-boson interactions. In the case where the mass imbalance between a boson and a fermion is negligible, supersymmetry within each reservoir is explicitly broken by the difference in two in-

*Contact author: zhangty@g.ecc.u-tokyo.ac.jp
†Contact author: guoyixin1997@g.ecc.u-tokyo.ac.jp
‡Contact author: htajima@g.ecc.u-tokyo.ac.jp
§Contact author: haozhao.liang@phys.s.u-tokyo.ac.jp

 

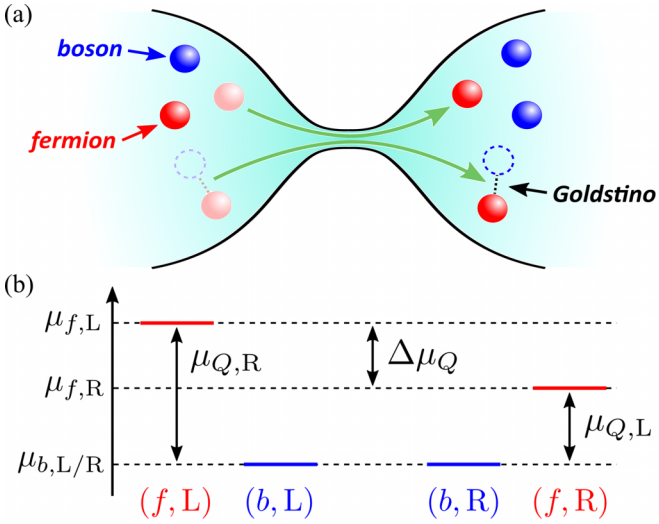


FIG. 1. (a) Schematic view of the two-terminal system considered in this work. Quasiparticle tunneling and supercharge tunneling are provoked by the chemical potential bias. The dashed circle represents the hole, and the pair of a fermion and a bosonic hole denotes a goldstino mode. (b) Chemical potentials for bosons (b) and fermions (f) in the left (L) and right (R) reservoirs, where $\mu_{Q,i}$ denotes the chemical potential for the supercharge. The bosonic chemical potentials in two reservoirs are set to be equal for suppressing the bosonic quasiparticle and pair tunneling processes.

teraction strengths and the chemical potential bias between bosons and fermions. Considering single-particle energy corrections for both bosons in the condensate and normal phases and adopting the Schwinger-Keldysh approach [53,54], we analyze the supersymmetric-like current, encompassing quasiparticle and goldstino contributions. Using a small mass-balanced mixture such as $^{173}$Yb - $^{174}$Yb, we present how the goldstino spectrum affects the tunneling transport.

This paper is structured as follows: In Sec. II, we introduce the Hamiltonian for the total system and the tunneling current operators. The formulas for supersymmetry-like tunneling currents are derived up to leading order in Sec. III. In Sec. IV, we explore the spectra and density of states for a goldstino in a given Bose-Fermi mixture and conduct numerical calculations for the supercharge tunneling current with varying chemical potential bias. Finally, a summary and perspectives are given in Sec. V.

Throughout the paper, we take $\hbar = k_{\mathrm{B}} = 1$ and the volumes of both reservoirs to be unity.

## II. FORMALISM

Here, we introduce the two-terminal model for tunneling between two Bose-Fermi mixtures separated by a potential barrier. The total Hamiltonian of the system is given by

$$\begin{aligned}\hat{H} = &\sum_{\alpha=f,b}\int d^3\boldsymbol{r}\hat{\psi}^\dagger_\alpha(\boldsymbol{r})\left[-\frac{\nabla^2}{2m_\alpha}+V_\alpha(\boldsymbol{r})\right]\hat{\psi}_\alpha(\boldsymbol{r})\\ &+\frac{U_{bb}}{2}\int d^3\boldsymbol{r}\hat{\psi}^\dagger_b(\boldsymbol{r})\hat{\psi}^\dagger_b(\boldsymbol{r})\hat{\psi}_b(\boldsymbol{r})\hat{\psi}_b(\boldsymbol{r})\\ &+U_{bf}\int d^3\boldsymbol{r}\hat{\psi}^\dagger_b(\boldsymbol{r})\hat{\psi}_b(\boldsymbol{r})\hat{\psi}^\dagger_f(\boldsymbol{r})\hat{\psi}_f(\boldsymbol{r}),\end{aligned} \tag{1}$$

where $\hat{\psi}_\alpha$ is the field operator of a fermion ($\alpha = f$) or a boson ($\alpha = b$). $m_\alpha$ are the masses of the fermion and boson. $V_\alpha(\boldsymbol{r})$ describes the potential barrier separating two reservoirs and goes to zero far away from the junction. $U_{bb}$ and $U_{bf}$ are, respectively, the coupling strengths for the boson-boson and boson-fermion interactions, which are characterized by the scattering lengths $a_{bb}$ and $a_{bf}$ as $U_{bb} = (4\pi a_{bb})/m_b$ and $U_{bf} = (2\pi a_{bf})/m_r$, with $m_r = 1/(1/m_b + 1/m_f)$ denoting the reduced mass.

For the steady-state transport between two reservoirs, the field operator can be decomposed as [55]

$$\hat{\psi}_\alpha(\boldsymbol{r}) = \hat{\psi}_{\alpha,\mathrm{L}}(\boldsymbol{r}) + \hat{\psi}_{\alpha,\mathrm{R}}(\boldsymbol{r}), \tag{2}$$

where $\hat{\psi}_{\alpha,i}(\boldsymbol{r})$ denotes the field operator in reservoir $i = \mathrm{L}, \mathrm{R}$. While the potential barrier peaking in the junction between the reservoirs induces an inhomogeneity near the barrier, in the far region the potential goes smoothly to zero. We can therefore consider uniform gases inside the reservoirs, with the wave function being the asymptotic form:

$$\psi_{\boldsymbol{k},\alpha,\mathrm{L}}(\boldsymbol{r}) = \begin{cases} e^{i\boldsymbol{k}\cdot\boldsymbol{r}} + R_{\boldsymbol{k},\alpha}e^{-i\boldsymbol{k}\cdot\boldsymbol{r}} & (x<0),\\ T_{\boldsymbol{k},\alpha}e^{i\boldsymbol{k}\cdot\boldsymbol{r}} & (x>0),\end{cases} \tag{3}$$

$$\psi_{\boldsymbol{k},\alpha,\mathrm{R}}(\boldsymbol{r}) = \begin{cases} T_{\boldsymbol{k},\alpha}e^{-i\boldsymbol{k}\cdot\boldsymbol{r}} & (x<0),\\ e^{-i\boldsymbol{k}\cdot\boldsymbol{r}} + R_{\boldsymbol{k},\alpha}e^{i\boldsymbol{k}\cdot\boldsymbol{r}} & (x>0),\end{cases} \tag{4}$$

where $\boldsymbol{k}$ is the wave number. The potential scattering induces the one-particle reflection and transmission coefficients $\mathcal{R}_{\boldsymbol{k},\alpha}$ and $\mathcal{T}_{\boldsymbol{k},\alpha}$, respectively. In Eqs. (3) and (4), the coordinate $x$ symbolically denotes the direction perpendicular to the potential barrier located at $x = 0$. Using Eqs. (3) and (4), we expand $\hat{\psi}_{\alpha,i}(\boldsymbol{r})$ in Eq. (2) as

$$\hat{\psi}_{f,i}(\boldsymbol{r}) = \sum_{\boldsymbol{k}}\psi_{\boldsymbol{k},f,i}(\boldsymbol{r})\hat{f}_{\boldsymbol{k},i}, \tag{5}$$

$$\hat{\psi}_{b,i}(\boldsymbol{r}) = \sum_{\boldsymbol{k}}\psi_{\boldsymbol{k},b,i}(\boldsymbol{r})\hat{b}_{\boldsymbol{k},i}, \tag{6}$$

where $\hat{f}_{\boldsymbol{k},i}$ and $\hat{b}_{\boldsymbol{k},i}$ are annihilation operators of a fermion and a boson, respectively. By substituting Eqs. (5) and (6) into Eq. (2) and then Eq. (1), we obtain the Hamiltonian of the system as

$$\hat{H} = \hat{H}_{\mathrm{L}} + \hat{H}_{\mathrm{R}} + \hat{H}_{1\mathrm{t}} + \hat{H}_{2\mathrm{t}}, \tag{7}$$

where the reservoir Hamiltonian reads

$$\begin{aligned}\hat{H}_{i=\mathrm{L,R}} = &\sum_{\boldsymbol{k}}\varepsilon_{\boldsymbol{k},f}\hat{f}^\dagger_{\boldsymbol{k},i}\hat{f}_{\boldsymbol{k},i} + \sum_{\boldsymbol{k}}\varepsilon_{\boldsymbol{k},b}\hat{b}^\dagger_{\boldsymbol{k},i}\hat{b}_{\boldsymbol{k},i}\\ &+\frac{U_{bb}}{2}\sum_{\boldsymbol{P},\boldsymbol{q},\boldsymbol{q}'}\hat{b}^\dagger_{\frac{\boldsymbol{P}}{2}+\boldsymbol{q},i}\hat{b}^\dagger_{\frac{\boldsymbol{P}}{2}-\boldsymbol{q},i}\hat{b}_{\frac{\boldsymbol{P}}{2}-\boldsymbol{q}',i}\hat{b}_{\frac{\boldsymbol{P}}{2}+\boldsymbol{q}',i}\\ &+U_{bf}\sum_{\boldsymbol{P},\boldsymbol{q},\boldsymbol{q}'}\hat{b}^\dagger_{\frac{\boldsymbol{P}}{2}+\boldsymbol{q},i}\hat{f}^\dagger_{\frac{\boldsymbol{P}}{2}-\boldsymbol{q},i}\hat{f}_{\frac{\boldsymbol{P}}{2}-\boldsymbol{q}',i}\hat{b}_{\frac{\boldsymbol{P}}{2}+\boldsymbol{q}',i},\end{aligned} \tag{8}$$

with the single-particle energy defined as $\varepsilon_{\boldsymbol{p},\alpha=b,f} = p^2/(2m_\alpha)$. This Hamiltonian includes the single-particle terms (the first line on the right-hand side), the boson-boson interaction term (the second line), and the boson-fermion interaction term (the third line). The one-body tunneling

Hamiltonian yields

$$\hat{H}_{1t} = \sum_{\boldsymbol{k}_1,\boldsymbol{k}_2} \mathcal{T}_{\boldsymbol{k}_1,\boldsymbol{k}_2,f}[\hat{f}^\dagger_{\boldsymbol{k}_1,\mathrm{L}}\hat{f}_{\boldsymbol{k}_2,\mathrm{R}} + \hat{f}^\dagger_{\boldsymbol{k}_1,\mathrm{R}}\hat{f}_{\boldsymbol{k}_2,\mathrm{L}}] + \sum_{\boldsymbol{k}_1,\boldsymbol{k}_2} \mathcal{T}_{\boldsymbol{k}_1,\boldsymbol{k}_2,b}[\hat{b}^\dagger_{\boldsymbol{k}_1,\mathrm{L}}\hat{b}_{\boldsymbol{k}_2,\mathrm{R}} + \hat{b}^\dagger_{\boldsymbol{k}_1,\mathrm{R}}\hat{b}_{\boldsymbol{k}_2,\mathrm{L}}], \tag{9}$$

which is associated with the potential barrier. The one-body tunneling amplitudes are given by

$$\mathcal{T}_{\boldsymbol{k}_1,\boldsymbol{k}_2,f} = \mathcal{C}_{\boldsymbol{k}_1,\boldsymbol{k}_2,f}\left[\delta_{\boldsymbol{k}_1,\boldsymbol{k}_2}\varepsilon_{\boldsymbol{k}_1,f} + V_f(\boldsymbol{k}_1-\boldsymbol{k}_2) + \frac{U_{fb}}{2}\sum_i \hat{N}_{b,\boldsymbol{k}_1-\boldsymbol{k}_2,i}\right], \tag{10a}$$

$$\mathcal{T}_{\boldsymbol{k}_1,\boldsymbol{k}_2,b} = \mathcal{C}_{\boldsymbol{k}_1,\boldsymbol{k}_2,b}\left[\delta_{\boldsymbol{k}_1,\boldsymbol{k}_2}\varepsilon_{\boldsymbol{k}_1,b} + V_b(\boldsymbol{k}_1-\boldsymbol{k}_2) + \frac{U_{bb}}{2}\sum_i \hat{N}_{b,\boldsymbol{k}_1-\boldsymbol{k}_2,i} + \frac{U_{bf}}{2}\sum_i \hat{N}_{f,\boldsymbol{k}_1-\boldsymbol{k}_2,i}\right], \tag{10b}$$

where $\hat{N}_{\alpha,\boldsymbol{k},i}$ is the density operator in the reservoir $i$. We define $\mathcal{C}_{\boldsymbol{k}_1,\boldsymbol{k}_2,\alpha} = \int d^3\boldsymbol{r}\,\psi^*_{\boldsymbol{k}_1,\alpha,\mathrm{L}}(\boldsymbol{r})\psi_{\boldsymbol{k}_2,\alpha,\mathrm{R}}(\boldsymbol{r})$ as the overlap integral of wave functions between two reservoirs, which is proportional to the transmission coefficient $\mathcal{T}_{\boldsymbol{k},\alpha}$ in Eqs. (3) and (4). Note that $V_\alpha(\boldsymbol{k})$ is the Fourier transformed potential barrier, which yields a constant $V_{0,\alpha}$ because we approximately use a delta function for the barrier $V_\alpha(x) = V_{0,\alpha}\delta(x/\lambda)$, where $\lambda$ is a typical length scale of the barrier width.

The two-body tunneling Hamiltonian can be written as the sum of three terms, $\hat{H}_{2t} = \hat{H}_{bb} + \hat{H}_{bf} + \hat{H}_Q$, corresponding to the tunneling of boson-boson pairs, boson-fermion pairs, and supercharges, respectively . The pair tunneling terms read

$$\hat{H}_{bb} = \frac{1}{2}\mathcal{G}_{bb}\sum_{\boldsymbol{p},\boldsymbol{q}}[\hat{P}^\dagger_{bb,\mathrm{L}}(\boldsymbol{p})\hat{P}_{bb,\mathrm{R}}(\boldsymbol{q}) + \mathrm{H.c.}], \tag{11a}$$

$$\hat{H}_{bf} = \mathcal{G}_{bf}\sum_{\boldsymbol{p},\boldsymbol{q}}[\hat{P}^\dagger_{bf,\mathrm{L}}(\boldsymbol{p})\hat{P}_{bf,\mathrm{R}}(\boldsymbol{q}) + \mathrm{H.c.}], \tag{11b}$$

where $\hat{P}_{bb,i}$ and $\hat{P}_{bf,i}$ are, respectively, the annihilation operators for a boson-boson pair and a boson-fermion pair, while $\mathcal{G}_{bb}$ and $\mathcal{G}_{bf}$ are the pair tunneling amplitudes.

Now we introduce the supercharge operator $\hat{Q}$ and $\hat{Q}^\dagger$, which are generators of supersymmetry transformations [56]. They can be defined in second quantized notation as

$$\hat{Q}_i(\boldsymbol{p}) = \sum_{\boldsymbol{k}} \hat{f}_{\boldsymbol{k},i}\hat{b}^\dagger_{\boldsymbol{k}-\boldsymbol{p},i}, \quad \hat{Q}^\dagger_i(\boldsymbol{p}) = \sum_{\boldsymbol{k}} \hat{b}_{\boldsymbol{k}-\boldsymbol{p},i}\hat{f}^\dagger_{\boldsymbol{k},i}. \tag{12}$$

The supercharge operators satisfy the following relations: $\hat{Q}_i^2 = (\hat{Q}_i^\dagger)^2 = 0$, $\{\hat{Q}_i, \hat{Q}_i^\dagger\} = \hat{N}_i = \hat{N}_{b,i} + \hat{N}_{f,i}$, and $[\hat{Q}_i, \hat{N}_i] = [\hat{Q}_i^\dagger, \hat{N}_i] = 0$, and thus, they are fermionic operators. Here, $\hat{N}_{f,i} = \sum_{\boldsymbol{p}} \hat{f}^\dagger_{\boldsymbol{p},i}\hat{f}_{\boldsymbol{p},i}$ and $\hat{N}_{b,i} = \sum_{\boldsymbol{p}} \hat{b}^\dagger_{\boldsymbol{p},i}\hat{b}_{\boldsymbol{p},i}$ are the particle numbers of fermions and bosons in reservoir $i$. Physically, $\hat{Q}$ changes a fermion into a boson, while $\hat{Q}^\dagger$ does the opposite. The supercharge tunneling term can then be written as

$$H_Q = \mathcal{G}_Q\sum_{\boldsymbol{p},\boldsymbol{q}}[\hat{Q}^\dagger_{\mathrm{L}}(\boldsymbol{p})\hat{Q}_{\mathrm{R}}(\boldsymbol{q}) + \mathrm{H.c.}], \tag{13}$$

with the tunneling amplitude $\mathcal{G}_Q$. Taking the long-wavelength limit for the transmitted waves, the amplitudes of the two-body tunneling terms are given by $\mathcal{G}_{bb} = U_{bb}\,\mathrm{Re}[T^2_{\boldsymbol{0},b}]$, $\mathcal{G}_{bf} = U_{bf}\,\mathrm{Re}[T_{\boldsymbol{0},b}T_{\boldsymbol{0},f}]$, and $\mathcal{G}_Q = U_{bf}\,\mathrm{Re}[T_{\boldsymbol{0},b}T^*_{\boldsymbol{0},f}]$ [55,57]. Note that we consider the effective Hamiltonian for the system where we omit the particle reflection and the induced interface interaction, which are irrelevant to our study.

The supersymmetry-like current operator is given by

$$\hat{I}_{\mathrm{SUSY}} = i[\hat{N}_{b,\mathrm{L}} - \hat{N}_{f,\mathrm{L}}, \hat{H}]. \tag{14}$$

It can be rewritten as $\hat{I}_{\mathrm{SUSY}} = \hat{I}_{1t} + \hat{I}_{bb} + \hat{I}_{bf} + \hat{I}_Q$, with the quasiparticle tunneling, boson-boson pair tunneling, boson-fermion pair tunneling, and supercharge tunneling contributions being

$$\hat{I}_{1t} = i\sum_{\boldsymbol{p},\boldsymbol{q}}[\mathcal{T}_f(\hat{f}^\dagger_{\boldsymbol{p},\mathrm{R}}\hat{f}_{\boldsymbol{q},\mathrm{L}} - \hat{f}^\dagger_{\boldsymbol{p},\mathrm{L}}\hat{f}_{\boldsymbol{q},\mathrm{R}}) + \mathcal{T}_b(\hat{b}^\dagger_{\boldsymbol{p},\mathrm{L}}\hat{b}_{\boldsymbol{q},\mathrm{R}} - \hat{b}^\dagger_{\boldsymbol{p},\mathrm{R}}\hat{b}_{\boldsymbol{q},\mathrm{L}})], \tag{15}$$

$$\hat{I}_{bb} = i\mathcal{G}_{bb}\sum_{\boldsymbol{p},\boldsymbol{q}}\hat{P}^\dagger_{bb,\mathrm{L}}(\boldsymbol{p})\hat{P}_{bb,\mathrm{R}}(\boldsymbol{q}) + \mathrm{H.c.}, \tag{16}$$

$$\hat{I}_{bf} = 2i\mathcal{G}_{bf}\sum_{\boldsymbol{p},\boldsymbol{q}}\hat{P}^\dagger_{bf,\mathrm{L}}(\boldsymbol{p})\hat{P}_{bf,\mathrm{R}}(\boldsymbol{q}) + \mathrm{H.c.}, \tag{17}$$

$$\hat{I}_Q = 2i\mathcal{G}_Q\sum_{\boldsymbol{p},\boldsymbol{q}}\hat{Q}^\dagger_{\mathrm{L}}(\boldsymbol{p})\hat{Q}_{\mathrm{R}}(\boldsymbol{q}) + \mathrm{H.c.}, \tag{18}$$

respectively. Here, we approximately use the momentum-independent one-body tunneling amplitudes $\mathcal{T}_f = \mathcal{C}_{0,0,f}(\epsilon_{\mathrm{F}} + V_{0,f})$ and $\mathcal{T}_b = \mathcal{C}_{0,0,b}(\epsilon_b + V_{0,b})$, which correspond to the momentum-conserved tunnelings near the Fermi energy $\epsilon_{\mathrm{F}} = (6\pi^2 N_f)^{2/3}/(2m_f)$ and the bosonic energy scale $\epsilon_b = (6\pi^2 N_b)^{2/3}/(2m_b)$, with the transmission coefficient at long-wavelength limit ($\boldsymbol{k} \to 0$). $N_\alpha = \langle\hat{N}_{\alpha,\mathrm{L}}\rangle$ is the statistical average of the particle numbers in reservoir L. A similar two-terminal model was applied to study the mass current and spin current in strongly correlated Fermi gases [50,55,58]. On the one hand, the supercharge tunneling can be regarded as an analog of the spin-flip process if we replace the supercharge operators with spin ladder operators. Physically, the interchange of a fermion and a boson corresponds to the interchange of spin-up and spin-down particles in a two-component Fermi gas. On the other hand, the spin-ladder operators involve the bosonic commutation relations, in contrast to the fermionic supercharge operator $Q$. Such a difference in the operator properties leads to the different distribution functions in the tunneling current.

## III. SUPERSYMMETRY-LIKE CURRENT

Using the current operator in the Heisenberg picture, in this section we derive the formulas for the supersymmetry-like currents by applying the Schwinger-Keldysh approach. Taking the tunneling Hamiltonian as a perturbation term, the expectation value of current can be expanded as

$$I_{\mathrm{SUSY}}(t,t') = \sum_{n=0}^{\infty}\frac{(-i)^n}{n!}\int_C dt_1\cdots\int_C dt_n \langle T_C\hat{I}_{\mathrm{SUSY}}(t,t')\hat{H}_{\mathrm{t}}(t_1)\cdots\hat{H}_{\mathrm{t}}(t_n)\rangle, \tag{19}$$

where $\hat{H}_{\mathrm{t}} = \hat{H}_{1t} + \hat{H}_{2t}$. The time integral is performed over the Keldysh contour $C$, comprising both a backward and a

forward branch, with $T_C$ denoting the contour-time-ordering product. The time arguments on different branches are distinguished by the notations $t$ and $t'$. It is important to note that the Schwinger-Keldysh formalism is well suited for describing nonequilibrium systems, where operators evolve in the interaction picture with the Hamiltonian $\hat{H}_0 = \sum_{\boldsymbol{k},i} \varepsilon_{\boldsymbol{k},f} \hat{f}^\dagger_{\boldsymbol{k},i} \hat{f}_{\boldsymbol{k},i} + \sum_{\boldsymbol{k},i} \varepsilon_{\boldsymbol{k},b} \hat{b}^\dagger_{\boldsymbol{k},i} \hat{b}_{\boldsymbol{k},i}$. We assume local equilibrium within each reservoir described by the chemical potential $\mu_{\alpha,i}$, where operators evolve according to the grand-canonical Hamiltonian $\hat{K}_0 = \hat{H}_0 - \mu_{f,i}\hat{N}_{f,i} - \mu_{b,i}\hat{N}_{b,i}$. Consequently, we perform a transformation on the creation and annihilation operators: $\hat{f}^\dagger_{\boldsymbol{k},i}(t) \to e^{i\mu_{f,i}t}\hat{f}^\dagger_{\boldsymbol{k},i}(t)$, $\hat{f}_{\boldsymbol{k},i}(t) \to e^{-i\mu_{f,i}t}\hat{f}_{\boldsymbol{k},i}(t)$, $\hat{b}^\dagger_{\boldsymbol{k},i}(t) \to e^{i\mu_{b,i}t}\hat{b}^\dagger_{\boldsymbol{k},i}(t)$, and $\hat{b}_{\boldsymbol{k},i}(t) \to e^{-i\mu_{b,i}t}\hat{b}_{\boldsymbol{k},i}(t)$.

Applying the Langreth rule to convert the integral over the Keldysh contour to that over the real-time axis and subsequently performing the Fourier transform, we derive the expressions for the quasiparticle and pair tunneling contributions to the supersymmetry-like current while retaining the truncation at leading order,

$$\begin{aligned} I_{\rm lt} = {} & 4\mathcal{T}_f^2 \int \frac{d\omega}{2\pi} \sum_{\boldsymbol{p},\boldsymbol{q}} \mathrm{Im}\, G_{f,\boldsymbol{p},\mathrm{L}}(\omega - \Delta\mu_f)\, \mathrm{Im}\, G_{f,\boldsymbol{q},\mathrm{R}}(\omega) \\ & \times [f_f(\omega - \Delta\mu_f) - f_f(\omega)] \\ & - 4\mathcal{T}_b^2 \int \frac{d\omega}{2\pi} \sum_{\boldsymbol{p},\boldsymbol{q}} \mathrm{Im}\, G_{b,\boldsymbol{p},\mathrm{L}}(\omega - \Delta\mu_b)\, \mathrm{Im}\, G_{b,\boldsymbol{q},\mathrm{R}}(\omega) \\ & \times [f_b(\omega - \Delta\mu_b) - f_b(\omega)], \end{aligned} \tag{20}$$

$$\begin{aligned} I_{bb} = {} & 2\mathcal{G}_{bb}^2 \sum_{\boldsymbol{p},\boldsymbol{q}} \int \frac{d\Omega}{2\pi} \mathrm{Im}\, \Gamma_{bb,\boldsymbol{p},\mathrm{L}}(\Omega - 2\Delta\mu_b)\, \mathrm{Im}\, \Gamma_{bb,\boldsymbol{q},\mathrm{R}}(\Omega) \\ & \times [f_b(\Omega - 2\Delta\mu_b) - f_b(\Omega)], \end{aligned} \tag{21}$$

$$\begin{aligned} I_{bf} = {} & 8\mathcal{G}_{bf}^2 \sum_{\boldsymbol{p},\boldsymbol{q}} \int \frac{d\Omega}{2\pi} \mathrm{Im}\, \Gamma_{bf,\boldsymbol{p},\mathrm{L}}[\Omega - (\Delta\mu_f + \Delta\mu_b)] \\ & \times \mathrm{Im}\, \Gamma_{bf,\boldsymbol{q},\mathrm{R}}(\Omega)\{f_f(\Omega - [\Delta\mu_f + \Delta\mu_b)] - f_f(\Omega)\}. \end{aligned} \tag{22}$$

Here, $G_{\alpha,\boldsymbol{p},i}(\omega)$ and $\Gamma_{bb(bf),\boldsymbol{p},i}(\Omega)$ are, respectively, the Fourier decompositions of the retarded Green's functions for a single particle and pair, defined as $G_{\alpha,\boldsymbol{p},i}(t,t') = -i\theta(t-t')\langle\{\hat{\alpha}_{\boldsymbol{p},i}(t)\hat{\alpha}^\dagger_{\boldsymbol{p},i}(t')\}\rangle$ $(\hat{\alpha} = \hat{f}, \hat{b})$, $\Gamma_{bb,\boldsymbol{p},i}(t,t') = -i\theta(t-t')\langle[\hat{P}_{bb,\boldsymbol{p},i}(t)\hat{P}^\dagger_{bb,\boldsymbol{p},i}(t')]\rangle$, and $\Gamma_{bf,\boldsymbol{p},i}(t,t') = -i\theta(t-t')\langle\{\hat{P}_{bf,\boldsymbol{p},i}(t)\hat{P}^\dagger_{bf,\boldsymbol{p},i}(t')\}\rangle$, with brackets $[\cdots]$ and $\{\cdots\}$ denoting the commutation and anticommutation operations. The chemical potential bias is denoted as $\Delta\mu_\alpha = \mu_{\alpha,\mathrm{L}} - \mu_{\alpha,\mathrm{R}}$, and $f_\alpha(\omega)$ is the distribution function obtained from the relations between the lesser and retarded Green's functions: $G^<_\alpha(\omega) = \mp 2i\, \mathrm{Im}\, G_\alpha(\omega) f_\alpha(\omega)$ ($-$ for $\alpha = f$ and $+$ for $\alpha = b$) and $\Gamma^<_{bb(bf)}(\Omega) = \pm 2i\, \mathrm{Im}\, \Gamma_{bb(bf)}(\Omega) f_{b(f)}(\Omega)$.

We then introduce the goldstino propagator, which is defined as $\chi_{\boldsymbol{p}}(t,t') = i\theta(t-t')\langle\{\hat{Q}_{\boldsymbol{p}}(t), \hat{Q}^\dagger_{\boldsymbol{p}}(t')\}\rangle$ in the linear response theory. The relation between the lesser component and retarded one reads $\chi^<(\Omega) = -2i\, \mathrm{Im}\, \chi(\Omega) f_f(\Omega)$. If we define $\mu_{Q,i} = \mu_{f,i} - \mu_{b,i}$, the goldstino tunneling current can then be written as

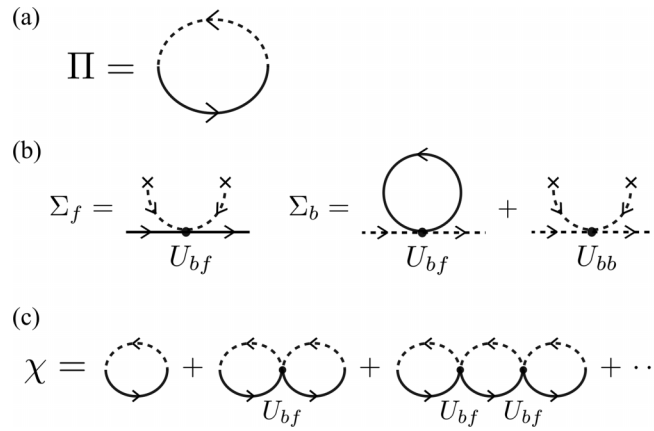


FIG. 2. (a) One-loop diagram for a noninteracting goldstino propagator. The solid (dashed) line represents the fermion (boson) propagator. (b) Diagrams of leading-order self-energies of fermions (the first one) and bosons (the second and third ones). The cross connected to one end of a dashed line denotes the contribution of the boson's condensate. (c) RPA calculations for the explicit propagator of the goldstino.

$$\begin{aligned} I_Q = {} & 8\mathcal{G}_Q^2 \sum_{\boldsymbol{p},\boldsymbol{q}} \int \frac{d\Omega}{2\pi} \mathrm{Im}\, \chi_{\boldsymbol{p},\mathrm{L}}(\Omega - \Delta\mu_Q)\, \mathrm{Im}\, \chi_{\boldsymbol{q},\mathrm{R}}(\Omega) \\ & \times [f_f(\Omega - \Delta\mu_Q) - f_f(\Omega)], \end{aligned} \tag{23}$$

with $\Delta\mu_Q = \mu_{Q,L} - \mu_{Q,R}$. To induce the supercharge tunneling current with $I_{\rm pair}$ suppressed, we shall take $\mu_{b,\mathrm{L}} = \mu_{b,\mathrm{R}}$ but different fermion chemical potentials in the two reservoirs.

## IV. NUMERICAL RESULTS

In order to search for evidence of the existence of the goldstino, in the following calculations, we concentrate on the supercharge tunneling current, neglecting the boson-fermion pair tunneling, which should be suppressed by the repulsive interaction between a boson and a fermion. It is noted that the repulsive quantum gas encounters an instability toward pair formation [59,60], which would compete with a phase separation in the strongly interacting regime [61]. Nevertheless, to avoid this we consider the weakly interacting case, where the two-particle boundary state is very deep and the Bose-Fermi mixture remains at a metastable equilibrium state, so that our approach is valid.

### A. Spectral functions in bulk reservoirs

First, we calculate the spectral functions in bulk reservoirs, and thus, we suppress the indices for the reservoirs ($i = \mathrm{L}, \mathrm{R}$) for convenience in this section. The one-loop diagram of the bare goldstino propagator $\Pi$ includes a fermion propagator and a boson propagator as drawn in Fig. 2(a). The explicit form of $\Pi_{\boldsymbol{p}}(\Omega)$ is given by

$$\Pi_{\boldsymbol{p}}(\Omega) = -\int \frac{d^3\boldsymbol{k}}{(2\pi)^3} \frac{f_f(\xi_{\boldsymbol{k}+\boldsymbol{p},f}) + f_b(\xi_{\boldsymbol{k},b})}{\Omega + i\delta - \xi_{\boldsymbol{k}+\boldsymbol{p},f} + \xi_{\boldsymbol{k},b}}. \tag{24}$$

Here, we define $\xi_{\boldsymbol{k},f} = \boldsymbol{k}^2/(2m_f) - \mu_f + \Sigma_f$ and $\xi_{\boldsymbol{k},b} = \boldsymbol{k}^2/(2m_b) - \mu_b + \Sigma_b$, where $\Sigma_f$ and $\Sigma_b$ denote the mean-field corrections for the single-particle energies of fermions and bosons. We consider the leading-order correction caused by the self-energies below the BEC critical temperature, as shown in Fig. 2(b), where the first diagram describes that of a fermion and the last two describe that of a boson. For fermions and bosons with nonzero momenta, the self-energies read $\Sigma_f = U_{bf}N_b$ and $\Sigma_b = 2U_{bb}N_b + U_{bf}N_f$, respectively. For condensed bosons, it turns out to be $\Sigma_{b,0} = U_{bb}N_b + U_{bf}N_f$ due to the absence of an exchange term in the former case [27]. The chemical potentials of bosons and fermions can be given as $\mu_b = dE/dN_b = U_{bb}N_b + U_{bf}N_f$ and $\mu_f = dE/dN_f = \epsilon_{\rm F} + U_{bf}N_b$. Accordingly, the Hugenholtz-Pines condition [62], that is, the gapless condition in the condensed phase, is fulfilled as $\xi_{\boldsymbol{k}=\boldsymbol{0},b} \equiv -\mu_b + \Sigma_{b,0} = 0$. However, for nonzero $\boldsymbol{k}$, the dispersion reads $\xi_{\boldsymbol{k},b} = k^2/(2m_b) + U_{bb}N_b$ [63] because the present approximation ignores the coupling with the holelike excitation given by $\hat{b}^\dagger_{\boldsymbol{k}}\hat{b}^\dagger_{-\boldsymbol{k}}$ and $\hat{b}_{-\boldsymbol{k}}\hat{b}_{\boldsymbol{k}}$, which can be justified at $|\boldsymbol{k}| \gtrsim \sqrt{2mU_{bb}N_b}$ [27]. Note that apart from the mean-field approach we apply in this paper, the quasiparticle spectra can be modified by beyond-mean-field theories [64]. In this regard, we consider the weak-coupling regime, where such corrections are small.

Taking the mass-balanced case $m_b = m_f = m$, we can rewrite the one-loop propagator as

$$\begin{aligned}\Pi_{\boldsymbol{p}}(\Omega) &= -\frac{N_b^0}{\Omega + \epsilon_{\rm F} + i\delta - \boldsymbol{p}^2/2m} \\ &\quad - \int \frac{d^3\boldsymbol{k}}{(2\pi)^3} \frac{f_f(\xi_{\boldsymbol{k}+\boldsymbol{p},f}) + f_b(\xi_{\boldsymbol{k},b})}{\Omega + i\delta - \xi_{\boldsymbol{k}+\boldsymbol{p},f} + \xi_{\boldsymbol{k},b}} \\ &= \Pi^{\rm p}_{\boldsymbol{p}}(\Omega) + \Pi^{\rm c}_{\boldsymbol{p}}(\Omega), \end{aligned} \tag{25}$$

where $N_b^0$ is the number of bosons in the condensate, $\xi_{\boldsymbol{k},f} = \boldsymbol{k}^2/2m - \epsilon_{\rm F}$, and $\xi_{\boldsymbol{k},b} = \boldsymbol{k}^2/2m + U_{bb}N_b$. $\Pi^{\rm p}$ and $\Pi^{\rm c}$ denote the contributions to the spectrum from the pole and continuum, respectively. When the temperature approaches zero, $N_b^0 \to N_b$, while the distribution of bosons with $k > 0$ vanishes, and

$$\Pi^{\rm c}_{\boldsymbol{p}}(\Omega) \to -\int \frac{d^3\boldsymbol{k}}{(2\pi)^3} \frac{f_f(\xi_{\boldsymbol{k}+\boldsymbol{p},f})}{\Omega + i\delta - \xi_{\boldsymbol{k}+\boldsymbol{p},f} + \xi_{\boldsymbol{k},b}}. \tag{26}$$

We then use the random phase approximation (RPA) to calculate the explicit result of the goldstino propagator in the interacting regime. From Eq. (24), we can see that the one-loop diagram for $\Pi$ has an order of magnitude $U^{-1}$, with $U$ denoting the magnitude of interaction strengths. We can draw a series of diagrams consisting of $\Pi$ [as shown in Fig. 2(c)] which have the same order of magnitude $U^{-1}$, as one loop contributes $U^{-1}$ and one dot contributes $U$. Thus, all of these diagrams should be summed, yielding

$$\chi_{\boldsymbol{p}}(\Omega) = \frac{\Pi_{\boldsymbol{p}}(\Omega)}{1 + U_{bf}\Pi_{\boldsymbol{p}}(\Omega)}. \tag{27}$$

Defining the dimensionless interaction strengths $\tilde{U}_{bf} = 2U_{bf}N_f/\epsilon_{\rm F} = 8a_{bf}k_{\rm F}/(3\pi)$ and $\tilde{U}_{bb} = 2U_{bb}N_f/\epsilon_{\rm F} = 8a_{bb}k_{\rm F}/(3\pi)$, with $\epsilon_{\rm F}$ and $k_{\rm F}$ denoting the Fermi energy and Fermi momentum of the fermions, we calculated the goldstino spectra in a $^{173}$Yb - $^{174}$Yb mixture, where the boson-fermion and boson-boson scattering lengths are precisely determined by experiments as $a_{bf} = 138.49a_0$ and $a_{bb} = 104.72a_0$ [39] ($a_0$ is the Bohr radius). Since the scattering lengths cannot be tuned via magnetic Feshbach resonances in a $^{173}$Yb - $^{174}$Yb mixture, $\tilde{U}_{bf}$ can be changed only by $k_{\rm F}$, namely, the density $N_f$. For a certain value of $\tilde{U}_{bf}$, the corresponding density is $N_f \simeq 1.04 \times 10^{-8}\tilde{U}_{bf}^3/a_0^3$. Figure 3 shows the spectra with different particle densities, where the particle numbers of the two components are taken to be $N_b = 2N_f$. The goldstino poles denoted by a sharp peak arise from the condensate of bosons and yield a nonzero energy gap, which is caused by the explicit supersymmetry breaking associated with the chemical potential bias between fermions and bosons. The sharp-peaked structure indicates its long lifetime collective excitation, which is reminiscent of the bulk dissipationless flow observed in a strongly interacting $^{23}$Na - $^{40}$K mixture [65]. As the interaction strength increases, the pole gradually separates from the continuum and completely leaves the continuum when $\tilde{U}_{bf} \simeq 0.3$. Note that in the repulsively interacting regime, bosons and fermions tend to be spatially separated beyond a critical interaction strength [66,67]. Such phase separation was recently studied in mass-imbalanced mixtures, where the phase separation occurs at the repulsive branch when $a_{bf}$ is tuned from a small positive value to resonance [68–70]. This process is similar to the Stoner ferromagnetic phase transition in two-spin-component Fermi gases [71,72]. To keep the stability of the mixture against the phase separation, we focus on the weak-coupling regime ($\tilde{U}_{bf} < 0.4$).

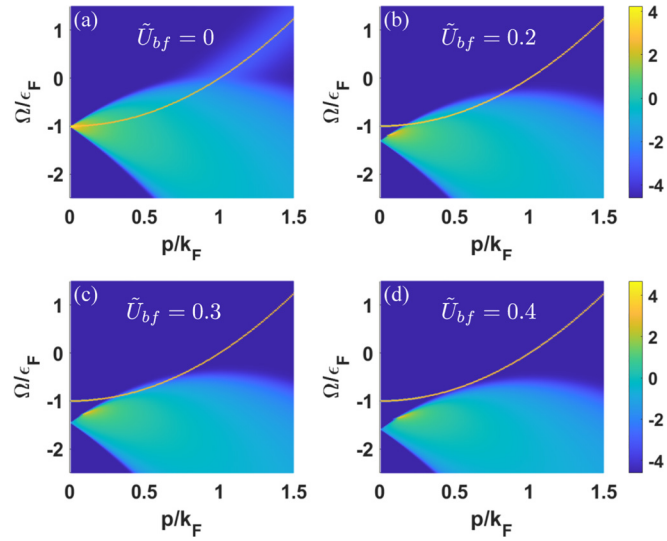


FIG. 3. Goldstino spectra with different particle densities in a Bose-Fermi mixture with explicitly broken supersymmetry. The color bars show the logarithmic scale. We fix the ratio $N_b/N_f = 2$, and the interaction parameters are chosen to be the experimental values of the $^{173}$Yb - $^{174}$Yb mixture, $a_{bf}/a_{bb} \simeq 1.32$. The goldstino poles (bright yellow line) originates from the BEC phase, and the continuum (light area) originates from the excitation of bosons. As density becomes larger, the poles start to separate from the continuum.

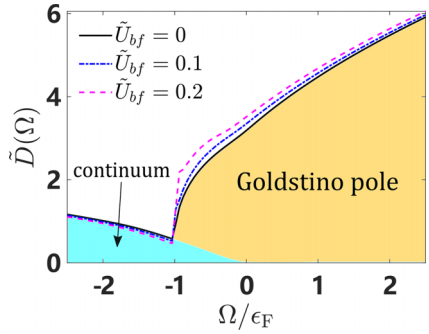


FIG. 4. Goldstino density of states with different particle number densities in a $^{173}$Yb - $^{174}$Yb mixture, where $\tilde{D}(\Omega) = \epsilon_F D(\Omega)/(6N_f^2)$. The boson-to-fermion particle number ratio is set to be $N_b/N_f = 2$.

It is useful to define the goldstino density of states (DOS) as

$$D(\Omega) = \sum_{\boldsymbol{p}} \mathrm{Im}\chi_{\boldsymbol{p}}(\Omega). \tag{28}$$

According to Eqs. (25) and (27), it consists of contributions from the poles and the continuum part, while that of the poles has a nonzero value only when $\Omega + \epsilon_F > 0$. We focus on the density below the critical point indicated by the goldstino spectrum at an extremely low temperature such that $N_b^0 \to N_b$ and Eq. (26) holds. Figure 4 shows the normalized goldstino DOS $\tilde{D}(\Omega)$ in a $^{173}$Yb - $^{174}$Yb mixture with different particle number densities and the fixed particle number ratio $N_{b,i}/N_{f,i} = 2$. We can see that when $\Omega > -\epsilon_F$, the contribution of the poles arises and dominates the DOS.

### B. Supercharge tunneling current

Using the DOS given by Eq. (28), one can rewrite the goldstino tunneling current Eq. (23) as

$$I_Q = 8\mathcal{G}_Q^2 \int \frac{d\Omega}{2\pi} D_L(\Omega - \Delta\mu_Q) D_R(\Omega) \times [f_f(\Omega - \Delta\mu_Q) - f_f(\Omega)]. \tag{29}$$

The bias dependence of $I_Q$ is shown in Fig. 5(a), where we consider the interaction parameters in the $^{173}$Yb - $^{174}$Yb mixture with the dimensionless interaction strength $\tilde{U}_{bf} = 0.2$. We notice that $I_Q$ increases monotonically with the chemical potential bias within the interval $0 < \Delta\mu_Q/\epsilon_F < 1$ but approaches a constant $I_Q/X_Q \simeq 6.3$ at $\Delta\mu_Q/\epsilon_F \geqslant 1$. This behavior indicates a vanishing differential conductance which is caused by the energy shift acting on the goldstino spectra by the large bias. Moreover, one can find asymmetric current-bias characteristics $I_Q(\Delta\mu_Q) \neq -I_Q(-\Delta\mu_Q)$. These features are distinct from the magnon-tunneling current [50,51] due to the statistical difference of the fermionic and bosonic Nambu-Goldstone modes. Indeed, the qualitative behavior of $I_Q$ is similar to that of the fermionic quasiparticle current $I_{1t}$ in Fig. 5(b); the analytical expression of $I_{1t}$ is shown in Appendix B.

From the expression of the chemical potentials at zero temperature, we find that $\Delta\mu_Q = \Delta\mu_f$ in the case of a balanced bosonic chemical potential. Accordingly, the goldstino pole energy is shifted by the change in the Fermi energy $\epsilon_{F,i} = \mu_{f,i} - U_{bb}N_{b,i}$ in each bulk reservoir. In this study, since we fix the Fermi energy in the left reservoir (i.e., $\epsilon_{F,L} \equiv \epsilon_F$), a nonzero $\Delta\mu_f$ leads to a shift of $\mu_{f,R} = \mu_{f,L} - \Delta\mu_f$ and thus the goldstino DOS in the right reservoir. Moreover, the energy shift $-\Delta\mu_Q$ is included in $D_L$ in Eq. (29), which leads to the same energy shift of the DOS in the left reservoir. Therefore, the energy shifts of goldstino poles in both reservoirs are equal to each other even as the bias increases. On the other hand, at extremely low temperature, the difference between the two distribution functions in Eq. (29) yields a nonzero interval $0 < \Omega < \Delta\mu_Q$. As a result, when the value of $\Delta\mu_Q/\epsilon_F$ exceeds 1, $I_Q$ saturates at a finite value due to the Fermi statistics of goldstino. This feature is similar to that of the quasiparticle tunneling current shown in Fig. 5(b), while the zero conductance of the latter is due to the zero chemical potential bias for the bosons that we choose. In spite of the similar behavior of these two tunneling signals, they may be distinguished through the current shot noise, which is proportional to the charge of the carriers and the average current [73,74]. The noise-to-current ratio is found to be a straightforward probe of tunneling channel [51,57], and it increases from 1 to 2 as the interaction strength is enhanced, indicating a crossover from one-body to multiparticle tunneling in an itinerant Fermi gas. Therefore, it is possible to find the dominant goldstino tunneling by measuring the noise and adjusting the interaction.

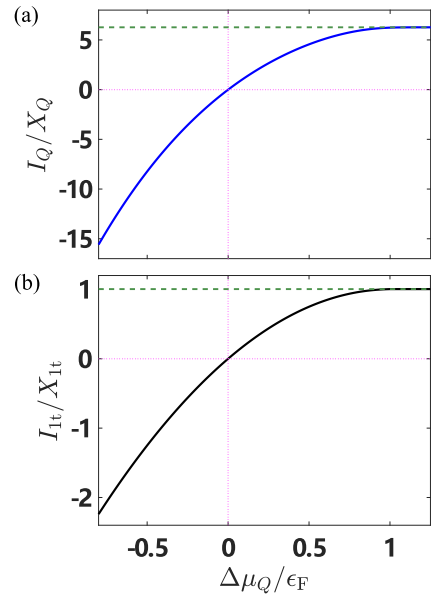


FIG. 5. (a) Bias dependence of the goldstino tunneling current in the $^{173}$Yb - $^{174}$Yb mixture. (b) Bias dependence of the quasiparticle current $I_{1t}$. Here, $X_Q = 9\mathcal{G}_Q^2(2N_{f,L})^4/(\epsilon_F\pi)$, and $X_{1t} = 9\pi\mathcal{T}_f^2 N_{f,L}^2/(4\epsilon_F)$ are normalizing factors of $I_Q$ and $I_{1t}$, respectively. We fix the Fermi energy for the left reservoir to be $\epsilon_F$. The ratio of particle numbers is fixed to be $N_{b,i}/N_{f,i} = 2$, and in both reservoirs the dimensionless interaction strength is taken to be $\tilde{U}_{bf} = 0.2$. The horizontal dotted lines in each panel represent the corresponding values at large $\Delta\mu_Q \to \infty$.

While the results presented above are specific to the $^{173}$Yb - $^{174}$Yb mixture, our methodology is applicable to other Bose-Fermi mixtures with small mass imbalances, such as $^{6}$Li - $^{7}$Li [13,14,37], $^{39}$K - $^{40}$K [38], $^{40}$K - $^{41}$K [15], $^{84}$Sr - $^{87}$Sr

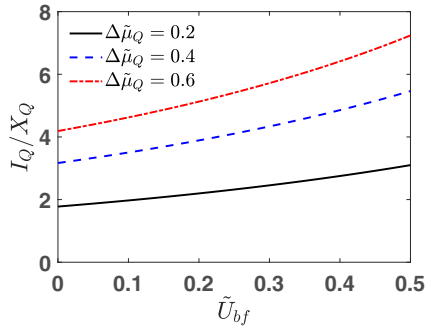


FIG. 6. Current-interaction features for the goldstino tunneling with different chemical potential biases. The boson-boson interaction strength is fixed to be $\tilde{U}_{bb} = 0.15$, while $\tilde{U}_{bf}$ is tuned from 0 to 0.5.

[39], $^{87}$Rb - $^{87}$Sr [16], and $^{161}$Dy - $^{162}$Dy [29], provided they are below their respective BEC temperatures. Additionally, in some of these mixtures, interactions between bosons or fermions can be adjusted by manipulating scattering lengths through magnetic Feshbach resonances [15,16,75–77]. This flexibility allows for exploring the goldstino's spectral features and its transport properties across various interaction strength regimes.

Motivated by this, we investigate the interaction dependence of the goldstino tunneling current, as shown in Fig. 6, where we fix the boson-boson interaction strength at $\tilde{U}_{bb} = 0.15$ and tune the boson-fermion interaction through a Feshbach resonance between species. We should note that although the beyond-mean-field theories demonstrate a $1/k^4$ tail for single-particle momentum distribution in short-range interacting regime [78–80], indicating that the quasiparticle tunneling current should be modified, we consider only the weak-coupling regime where the mean-field approximation can be employed and the $1/k^4$ momentum tail can be neglected. On the other hand, we can see from its expression [Eq. (20)] that while at finite temperature the quasiparticle tunneling would depend on the interaction due to the mean-field energy corrections, at extremely low temperatures the corrections are offset by the zero-temperature chemical potential, making $I_{1t}$ interaction independent. In contrast, the goldstino tunneling current is enhanced as the interaction strength increases even at zero temperature, providing a potential way to distinguish between these two signals. We should also note that the ratio between two normalizing factors is given by $X_Q/X_{1t} = 16\tilde{U}_{bf}^2\gamma^2/\pi^2$, where $\gamma = \frac{\epsilon_F}{U_{bf}}\frac{\mathcal{G}_Q}{\mathcal{T}_f}$ is a dimensionless ratio with an order of magnitude of $\gamma \sim 1$ [51]. Then combining this result with Fig. 5, we find that when $\tilde{U}_{bf}$ reaches around 0.3, $I_Q$ will have the same order of magnitude as $I_{1t}$, which means one can easily distinguish them with a relatively low accuracy of measurement.

Moreover, the shape of the potential barrier (e.g., height and width) can also influence $\mathcal{T}_f$ and $\mathcal{G}_Q$ through the modification of the transmission coefficients. While both one-body and two-body tunneling strengths decrease as the height and width increase, the latter is shown to be more sensitive to the barrier [51]. Such different dependences on the shape of the potential barrier may also aid in distinguishing the goldstino tunneling signal from the quasiparticle one.

## V. SUMMARY AND PERSPECTIVES

In this study, we theoretically examined the tunneling transport induced by a chemical potential bias in a Bose-Fermi mixture, which can be a promising route to detect the goldstino excitation associated with the broken supersymmetry in ultracold atomic experiments.

By calculating the goldstino spectrum and employing the Schwinger-Keldysh approach up to leading order, we explored the supersymmetry-like tunneling current through a two-terminal junction induced by a chemical potential bias between two reservoirs. The goldstino mode exhibits a chemical potential of $\mu_f - \mu_b$ and is found to contribute to the tunneling process. In spite of the similar bias dependence of the quasiparticle and goldstino tunneling currents, in Bose-Fermi mixtures allowing interaction tuning through Feshbach resonances, they may be distinguished through the interaction dependence.

Although the gapped goldstino excitation and its spectral properties have not been directly observed, our work suggests a potential avenue for probing them through tunneling transport, which can be conducted and detected in laboratories. Once the supercharge current is determined and agrees with the results of theoretical analysis, it will serve as strong evidence for the existence of the goldstino and supersymmetry in such Bose-Fermi mixed systems. Our approach can also be applied to other condensed matter systems exhibiting supersymmetric properties [81–83].

## ACKNOWLEDGMENTS

H.T. thanks Y. Hidaka and D. Satow for useful discussions. T.Z. and Y.G. were supported by the RIKEN Junior Research Associate Program. H.T. acknowledges the JSPS Grants-in-Aid for Scientific Research under Grants No. JP22H01158 and No. JP22K13981. H.L. acknowledges the JSPS Grant-in-Aid for Scientific Research (S) under Grant No. JP20H05648 and the RIKEN Pioneering Project: Evolution of Matter in the Universe.

T.Z. and Y.G. contributed equally to this paper.

## APPENDIX A: CALCULATION OF THE GOLDSTINO PROPAGATOR

In this Appendix, we give the details for calculating goldstino spectra. Note that the contribution of the continuum in Eq. (25) can be rewritten as

$$\Pi_{\boldsymbol{p}}^{c}(\Omega) = -\int \frac{d^3\boldsymbol{k}}{(2\pi)^3}\left[\frac{f_f(\xi_{\boldsymbol{k},f})}{\Omega + i\delta - \xi_{\boldsymbol{k},f} + \xi_{\boldsymbol{k}-\boldsymbol{p},b}} + \frac{f_b(\xi_{\boldsymbol{k},b})}{\Omega + i\delta - \xi_{\boldsymbol{k}+\boldsymbol{p},f} + \xi_{\boldsymbol{k},b}}\right]. \tag{A1}$$

We calculate the integral in a spherical coordinate system, where, according to the symmetry, we can take the vector $\boldsymbol{p}$ to be coincident with the $z$ axis. Taking $k_F$ and $\epsilon_F$ as the Fermi momentum and Fermi energy of the fermions, we define $\tilde{k} = k/k_F$, $\tilde{\Omega} = \Omega/\epsilon_F$, and $\tilde{\mu}_Q = \mu_Q/\epsilon_F$. Then after conducting the

angular integral, we have

$$\Pi^{\rm c}_{\boldsymbol{p}}(\Omega) = \frac{k_{\rm F}^3}{8\pi^2\epsilon_{\rm F}\tilde{p}}\int d\tilde{k}\tilde{k} \times\left[f_f(\xi_{\boldsymbol{k},f})\ln\left(\frac{\tilde{\Omega}+i\delta-2\tilde{k}\tilde{p}+\tilde{p}^2+\tilde{\mu}'_Q}{\tilde{\Omega}+i\delta+2\tilde{k}\tilde{p}+\tilde{p}^2+\tilde{\mu}'_Q}\right) + f_b(\xi_{\boldsymbol{k},b})\ln\left(\frac{\tilde{\Omega}+i\delta-2\tilde{k}\tilde{p}-\tilde{p}^2+\tilde{\mu}'_Q}{\tilde{\Omega}+i\delta+2\tilde{k}\tilde{p}-\tilde{p}^2+\tilde{\mu}'_Q}\right)\right], \tag{A2}$$

where $\mu'_Q = \mu_Q - (\Sigma_f - \Sigma_b) = \epsilon_{\rm F} + U_{bb}N_b$. Due to the infinitesimally small number $\delta$, the formulas inside the parentheses can be expressed as

$$\frac{\tilde{\Omega}+i\delta-2\tilde{k}\tilde{p}\pm\tilde{p}^2+\tilde{\mu}'_Q}{\tilde{\Omega}+i\delta+2\tilde{k}\tilde{p}\pm\tilde{p}^2+\tilde{\mu}'_Q} = \frac{|(\tilde{\Omega}\pm\tilde{p}^2+\tilde{\mu}'_Q)^2-4\tilde{k}^2\tilde{p}^2|}{(\tilde{\Omega}+2\tilde{k}\tilde{p}\pm\tilde{p}^2+\tilde{\mu}'_Q)^2} \times\exp\left\{i\arctan\left[\frac{4\tilde{k}\tilde{p}\delta}{(\tilde{\Omega}\pm\tilde{p}^2+\tilde{\mu}'_Q)^2-4\tilde{k}^2\tilde{p}^2}\right]\right\} = A^{\pm}_{\tilde{\boldsymbol{p}}}(\tilde{\Omega},\tilde{k})e^{i\tilde{\theta}^{\pm}_{\tilde{p}}(\tilde{\Omega},\tilde{k})}. \tag{A3}$$

Then we obtain the real part of the one-loop goldstino propagator:

$$\mathrm{Re}\,\Pi^{\rm c}_{\boldsymbol{p}}(\Omega) = \frac{3N_f}{4\epsilon_{\rm F}\tilde{p}}\int d\tilde{k}\,\tilde{k}\{f_f(\xi_{\boldsymbol{k},f})\ln[A^{+}_{\tilde{\boldsymbol{p}}}(\tilde{\Omega},\tilde{k})] + f_b(\xi_{\boldsymbol{k},b})\ln[A^{-}_{\tilde{\boldsymbol{p}}}(\tilde{\Omega},\tilde{k})]\}, \tag{A4}$$

where the fermionic density reads $N_f = k_{\rm F}^3/6\pi^2$. For the imaginary part of $\Pi$, according to the identity $\frac{1}{\Gamma+i\delta} = \mathcal{P}\frac{1}{\Gamma} - i\pi\delta(\Gamma)$, we have $\mathrm{Im}\,\Pi_{\boldsymbol{p}} = \mathrm{Im}\,\Pi^{\rm p}_{\boldsymbol{p}} + \mathrm{Im}\,\Pi^{\rm c}_{\boldsymbol{p}}$, where

$$\mathrm{Im}\,\Pi^{\rm p}_{\boldsymbol{p}}(\Omega) = \pi N_b^0\delta(\Omega+\epsilon_{\rm F}-\boldsymbol{p}^2/2m) \tag{A5}$$

and

$$\mathrm{Im}\,\Pi^{\rm c}_{\boldsymbol{p}}(\Omega) = \pi\int\frac{d^3\boldsymbol{k}}{(2\pi)^3}[f_f(\xi_{\boldsymbol{k}+\boldsymbol{p},f})+f_b(\xi_{\boldsymbol{k},b})]\,\delta[\Omega-(\boldsymbol{k}+\boldsymbol{p})^2/2m+\boldsymbol{k}^2/2m+\mu'_Q]. \tag{A6}$$

By expressing the integral over parameters in the spherical coordinates and performing a variable conversion, where $\cos\theta$ is replaced by $q = |\boldsymbol{k}+\boldsymbol{p}|$, and introducing parameters such as $\tilde{k}$ and $\tilde{\Omega}$, which are normalized by $k_{\rm F}$ and $\epsilon_{\rm F}$, the equation above can be reformulated as

$$\mathrm{Im}\,\Pi^{\rm c}_{\boldsymbol{p}}(\Omega) = \frac{k_{\rm F}^3}{4\pi\epsilon_{\rm F}\tilde{p}}\int\tilde{k}d\tilde{k}\int_{|\tilde{k}-\tilde{p}|}^{\tilde{k}+\tilde{p}}\tilde{q}d\tilde{q} \times[f_f(\xi_{\boldsymbol{q},f})+f_b(\xi_{\boldsymbol{k},b})]\delta(\tilde{\Omega}-\tilde{q}^2+\tilde{k}^2+\tilde{\mu}'_Q). \tag{A7}$$

By using the property of the delta function $\delta[f(x)] = \delta(x-x_0)/|f'(x_0)|$, with $f(x_0)=0$, we have

$$\mathrm{Im}\,\Pi^{\rm c}_{\boldsymbol{p}}(\Omega) = \frac{k_{\rm F}^3}{8\pi\epsilon_{\rm F}\tilde{p}}\int\tilde{k}d\tilde{k}\int_{|\tilde{k}-\tilde{p}|}^{\tilde{k}+\tilde{p}}d\tilde{q} \times[f_f(\xi_{\boldsymbol{q},f})+f_b(\xi_{\boldsymbol{k},b})]\delta(\tilde{q}-\tilde{q}_0), \tag{A8}$$

where $\tilde{q}_0 = \sqrt{\tilde{\Omega}+\tilde{k}^2+\tilde{\mu}'_Q}$. Meanwhile, for the integral to be nonzero, $\tilde{q}_0$ must satisfy the inequality $|\tilde{k}-\tilde{p}| \leqslant \tilde{q}_0 \leqslant \tilde{k}+\tilde{p}$, leading to a lower limit for the integral over $k$ as

$$\tilde{k} \geqslant \frac{1}{2}\left|\frac{\tilde{\Omega}+\tilde{\mu}'_Q}{\tilde{p}}-\tilde{p}\right|. \tag{A9}$$

Therefore, we obtain the expression for the imaginary part of the Lindhard function as given by

$$\mathrm{Im}\,\Pi^{\rm p}_{\boldsymbol{p}}(\Omega) = \pi N_b^0\delta(\Omega+\epsilon_{\rm F}-\boldsymbol{p}^2/2m), \tag{A10a}$$

$$\mathrm{Im}\,\Pi^{\rm c}_{\boldsymbol{p}}(\Omega) = \frac{3\pi N_f}{4\epsilon_{\rm F}\tilde{p}}\int_{\alpha}^{\infty}\tilde{k}d\tilde{k}[f_f(\xi_{q_0,f})+f_b(\xi_{k,b})], \tag{A10b}$$

where $\alpha = \frac{1}{2}|\frac{\tilde{\Omega}+\tilde{\mu}'_Q}{\tilde{p}}-\tilde{p}|$.

With the introduction of the dimensionless interaction strength $\tilde{U}_{ij} = 2U_{ij}N_f/\epsilon_{\rm F} = 8a_{ij}k_{\rm F}/(3\pi)$, the goldstino spectral function within the RPA can be computed as

$$\mathrm{Im}\,\tilde{\chi}_{\boldsymbol{p}}(\Omega) = \frac{\mathrm{Im}\,\tilde{\Pi}_{\boldsymbol{p}}(\Omega)}{\left[1+\tilde{U}_{bf}\,\mathrm{Re}\,\tilde{\Pi}^{\rm c}_{\boldsymbol{p}}(\Omega)\right]^2+\left[\tilde{U}_{bf}\,\mathrm{Im}\,\tilde{\Pi}^{\rm c}_{\boldsymbol{p}}(\Omega)\right]^2}, \tag{A11}$$

where $\tilde{\chi}_{\boldsymbol{p}} = \chi_{\boldsymbol{p}}\epsilon_{\rm F}/(2N_f)$ and $\tilde{\Pi}_{\boldsymbol{p},i} = \Pi_{\boldsymbol{p}}\epsilon_{\rm F}/(2N_f)$. The goldstino DOS can be calculated by changing the discrete summation in Eq. (28) into the integral over parameters in a spherical coordinate as

$$\tilde{D}(\Omega) = \int d\tilde{q}\tilde{q}^2\,\mathrm{Im}\,\tilde{\chi}^{\rm ret.}_{\boldsymbol{q}}(\Omega) = \Theta(\tilde{\Omega}+1)\frac{\pi N_b}{2N_f}\frac{\tilde{q}_0}{\left[1+\tilde{U}_{bf}\,\mathrm{Re}\,\tilde{\Pi}^{\rm c}_{q_0}(\Omega)\right]^2+\left[\tilde{U}_{bf}\,\mathrm{Im}\,\tilde{\Pi}^{\rm c}_{q_0}(\Omega)\right]^2} + \int d\tilde{q}\tilde{q}^2\frac{\mathrm{Im}\,\tilde{\Pi}^{\rm c}_{\boldsymbol{q}}(\Omega)}{\left[1+\tilde{U}_{bf}\,\mathrm{Re}\,\tilde{\Pi}^{\rm c}_{\boldsymbol{q}}(\Omega)\right]^2+\left[\tilde{U}_{bf}\,\mathrm{Im}\,\tilde{\Pi}^{\rm c}_{\boldsymbol{q}}(\Omega)\right]^2}, \tag{A12}$$

where $q_0 = \sqrt{2m(\Omega+\epsilon_{\rm F})}$. The first term on the right-hand side describes the contribution of the pole with a gap $\Delta_{\rm p} = -\epsilon_{\rm F}$, while the second one corresponds to that of the continuum.

Notice that in the denominator of Eq. (A11), we omit the contribution of $\Pi^{\rm p}$, whose spectrum is a delta function which does not affect the result of later integral calculations. We also omit the contribution of $\mathrm{Re}\,\Pi^{\rm p}$, which has a negligible

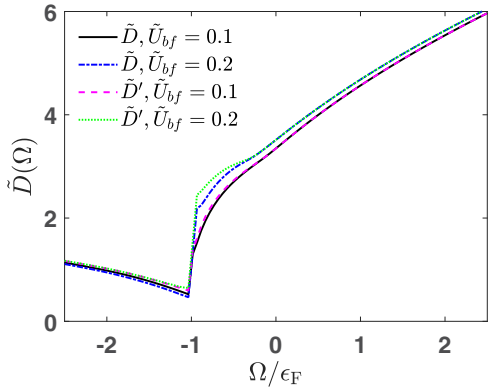


FIG. 7. Goldstino density of states with different particle number densities in a $^{173}$Yb - $^{174}$Yb mixture, where we compare the results taking Re $\Pi^{\mathrm{p}}$ into account ($\tilde{D}'$) with the results not taking Re $\Pi^{\mathrm{p}}$ into account ($\tilde{D}$). The boson-to-fermion particle number ratio is set to be $N_b/N_f = 2$.

effect on the goldstino density states in our weakly interacting regime, as shown in Fig. 7.

## APPENDIX B: CALCULATION OF THE QUASIPARTICLE TUNNELING CURRENT

In this Appendix, we provide the analytical derivations of the quasiparticle tunneling current $I_{1t}$ to understand the asymmetric characteristic clearly.

The Green's function of a single fermion at zero temperature is given by

$$G_{f,\boldsymbol{k}}(\omega) = \frac{1}{\omega - \xi_{\boldsymbol{k},f} + i\delta}, \tag{B1}$$

where $\xi_{\boldsymbol{k},f} = \boldsymbol{k}^2/2m - \epsilon_{\mathrm{F}}$ is the single-particle energy of fermions in the grand-canonical ensemble after taking into account the self-energy correction. Its imaginary part reads

$$\mathrm{Im}\, G_{f,\boldsymbol{k}}(\omega) = -\pi\delta(\omega - \xi_{\boldsymbol{k},f}). \tag{B2}$$

According to Eq. (20), the quasiparticle current can then be rewritten as

$$I_{1t} = 4\mathcal{T}_f^2 \int \frac{d\omega}{2\pi} \int \frac{d^3\boldsymbol{p}}{(2\pi)^3} \int \frac{d^3\boldsymbol{q}}{(2\pi)^3} \pi^2 \delta(\omega - \xi_{\boldsymbol{p},f,\mathrm{L}} - \Delta\mu_f) \times \delta(\omega - \xi_{\boldsymbol{q},f,\mathrm{R}})[f_f(\omega - \Delta\mu_f) - f_f(\Omega)]. \tag{B3}$$

In ultracold regimes, the Fermi distribution function can be approximately regarded as $f_f(\omega) \simeq \theta(-\omega)$. Fixing the Fermi energy of the left reservoir to be $\epsilon_{\mathrm{F}}$, we have

$$\begin{aligned} I_{1t} &\simeq \frac{\mathcal{T}_f^2 k_{\mathrm{F}}^6}{8\pi^3\epsilon_{\mathrm{F}}} \int d\tilde{\omega} \sqrt{\tilde{\omega} + 1 - \Delta\tilde{\mu}_f} \sqrt{\tilde{\omega} + 1 - \Delta\tilde{\mu}_f} \\ &\quad \times \theta(\tilde{\omega} + 1 - \Delta\tilde{\mu}_f)[\theta(\Delta\tilde{\mu}_f - \tilde{\omega}) - \theta(-\tilde{\omega})] \\ &= \frac{\mathcal{T}_f^2 k_{\mathrm{F}}^6}{8\pi^3\epsilon_{\mathrm{F}}} \int_0^{\Delta\tilde{\mu}_f} d\tilde{\omega}(\tilde{\omega} + 1 - \Delta\tilde{\mu}_f)\theta(\tilde{\omega} + 1 - \Delta\tilde{\mu}_f) \\ &= X_{1t}\{[(\tilde{\omega} + 1 - \Delta\tilde{\mu}_f)^2]_0^{\Delta\tilde{\mu}_f}\theta(1 - \Delta\tilde{\mu}_f) \\ &\quad + [(\tilde{\omega} + 1 - \Delta\tilde{\mu}_f)^2]_{\Delta\tilde{\mu}_f - 1}^{\Delta\tilde{\mu}_f}\theta(\Delta\tilde{\mu}_f - 1)\} \\ &= X_{1t}\big[1 - (1 - \Delta\tilde{\mu}_f)^2\theta(1 - \Delta\tilde{\mu}_f)\big], \end{aligned} \tag{B4}$$

where $\Delta\tilde{\mu}_f = \Delta\mu_f/\epsilon_{\mathrm{F}}$. In the present case with the balanced bosonic chemical potential in the two reservoirs, one can find $\Delta\mu_f = \Delta\mu_Q$.

From the derivation above, we can see that the asymmetric characteristic arises from the fixed Fermi energy in the left reservoir, while the vanishing differential conductance is due to the disappearance of the Fermi energy in the right reservoir.


[1] C. Chin, R. Grimm, P. Julienne, and E. Tiesinga, Feshbach resonances in ultracold gases, Rev. Mod. Phys. **82**, 1225 (2010).

[2] C.-C. Chien, S. Peotta, and M. Di Ventra, Quantum transport in ultracold atoms, Nat. Phys. **11**, 998 (2015).

[3] A. Sommer, M. Ku, G. Roati, and M. W. Zwierlein, Universal spin transport in a strongly interacting Fermi gas, Nature (London) **472**, 201 (2011).

[4] S. Krinner, M. Lebrat, D. Husmann, C. Grenier, J.-P. Brantut, and T. Esslinger, Mapping out spin and particle conductances in a quantum point contact, Proc. Natl. Acad. Sci. USA **113**, 8144 (2016).

[5] T. Enss, Transverse spin diffusion in strongly interacting Fermi gases, Phys. Rev. A **88**, 033630 (2013).

[6] T. Enss and J. H. Thywissen, Universal spin transport and quantum bounds for unitary fermions, Annu. Rev. Condens. Matter Phys. **10**, 85 (2019).

[7] A. B. Bardon, S. Beattie, C. Luciuk, W. Cairncross, D. Fine, N. S. Cheng, G. J. A. Edge, E. Taylor, S. Zhang, S. Trotzky, and J. H. Thywissen, Transverse demagnetization dynamics of a unitary Fermi gas, Science **344**, 722 (2014).

[8] D. Husmann, S. Uchino, S. Krinner, M. Lebrat, T. Giamarchi, T. Esslinger, and J.-P. Brantut, Connecting strongly correlated superfluids by a quantum point contact, Science **350**, 1498 (2015).

[9] G. Valtolina, A. Burchianti, A. Amico, E. Neri, K. Xhani, J. A. Seman, A. Trombettoni, A. Smerzi, M. Zaccanti, M. Inguscio, and G. Roati, Josephson effect in fermionic superfluids across the BEC-BCS crossover, Science **350**, 1505 (2015).

[10] S. Krinner, T. Esslinger, and J.-P. Brantut, Two-terminal transport measurements with cold atoms, J. Phys.: Condens. Matter **29**, 343003 (2017).

[11] W. J. Kwon, G. D. Pace, R. Panza, M. Inguscio, W. Zwerger, M. Zaccanti, F. Scazza, and G. Roati, Strongly correlated superfluid order parameters from dc Josephson supercurrents, Science **369**, 84 (2020).

[12] M. Bukov, Bose-Fermi mixtures: A mean-field study, Ph.D. thesis, Ludwig Maximilian University of Munich (LMU Munich), 2013.

[13] T. Ikemachi, A. Ito, Y. Aratake, Y. Chen, M. Koashi, M. Kuwata-Gonokami, and M. Horikoshi, All-optical production

of dual Bose–Einstein condensates of paired fermions and bosons with $^{6}$Li and $^{7}$Li, J. Phys. B **50**, 01LT01 (2017).

[14] S. Laurent, M. Pierce, M. Delehaye, T. Yefsah, F. Chevy, and C. Salomon, Connecting few-body inelastic decay to quantum correlations in a many-body system: A weakly coupled impurity in a resonant Fermi gas, Phys. Rev. Lett. **118**, 103403 (2017).

[15] C.-H. Wu, I. Santiago, J. W. Park, P. Ahmadi, and M. W. Zwierlein, Strongly interacting isotopic Bose-Fermi mixture immersed in a Fermi sea, Phys. Rev. A **84**, 011601(R) (2011).

[16] V. Barbé, A. Ciamei, B. Pasquiou, L. Reichsöllner, F. Schreck, P. S. Żuchowski, and J. M. Hutson, Observation of Feshbach resonances between alkali and closed-shell atoms, Nat. Phys. **14**, 881 (2018).

[17] K. K. Das, Bose-Fermi mixtures in one dimension, Phys. Rev. Lett. **90**, 170403 (2003).

[18] M. Lewenstein, L. Santos, M. A. Baranov, and H. Fehrmann, Atomic Bose-Fermi mixtures in an optical lattice, Phys. Rev. Lett. **92**, 050401 (2004).

[19] K. Günter, T. Stöferle, H. Moritz, M. Köhl, and T. Esslinger, Bose-Fermi mixtures in a three-dimensional optical lattice, Phys. Rev. Lett. **96**, 180402 (2006).

[20] P.-T. Qi and W.-S. Duan, Tunneling dynamics and phase transition of a Bose-Fermi mixture in a double well, Phys. Rev. A **84**, 033627 (2011).

[21] S. Wang, X. Yin, Y.-Y. Chen, Y. Zhang, and X.-W. Guan, Emergent ballistic transport of Bose–Fermi mixtures in one dimension, J. Phys. A **53**, 464002 (2020).

[22] Y. Yu and K. Yang, Supersymmetry and the goldstino-like mode in Bose-Fermi mixtures, Phys. Rev. Lett. **100**, 090404 (2008).

[23] T. Shi, Y. Yu, and C. P. Sun, Supersymmetric response of a Bose-Fermi mixture to photoassociation, Phys. Rev. A **81**, 011604(R) (2010).

[24] H.-H. Lai and K. Yang, Relaxation of a goldstino-like mode due to supersymmetry breaking in Bose-Fermi mixtures, Phys. Rev. A **91**, 063620 (2015).

[25] J.-P. Blaizot, Y. Hidaka, and D. Satow, Spectral properties of the goldstino in supersymmetric Bose-Fermi mixtures, Phys. Rev. A **92**, 063629 (2015).

[26] B. Bradlyn and A. Gromov, Supersymmetric waves in Bose-Fermi mixtures, Phys. Rev. A **93**, 033642 (2016).

[27] J.-P. Blaizot, Y. Hidaka, and D. Satow, Goldstino in supersymmetric Bose-Fermi mixtures in the presence of a Bose-Einstein condensate, Phys. Rev. A **96**, 063617 (2017).

[28] H. Tajima, Y. Hidaka, and D. Satow, Goldstino spectrum in an ultracold Bose-Fermi mixture with explicitly broken supersymmetry, Phys. Rev. Res. **3**, 013035 (2021).

[29] K. Maeda, G. Baym, and T. Hatsuda, Simulating dense QCD matter with ultracold atomic boson-fermion mixtures, Phys. Rev. Lett. **103**, 085301 (2009).

[30] G. Baym, T. Hatsuda, T. Kojo, P. D. Powell, Y. Song, and T. Takatsuka, From hadrons to quarks in neutron stars: A review, Rep. Prog. Phys. **81**, 056902 (2018).

[31] K. Manabe and Y. Ohashi, Thermodynamic stability, compressibility matrices, and effects of mediated interactions in a strongly interacting Bose-Fermi mixture, Phys. Rev. A **103**, 063317 (2021).

[32] Y. Guo, H. Tajima, T. Hatsuda, and H. Liang, BCS-BCS crossover between atomic and molecular superfluids in a Bose-Fermi mixture, Phys. Rev. A **108**, 023304 (2023).

[33] T. Sogo, T. Miyakawa, T. Suzuki, and H. Yabu, RPA study of collective oscillations in the Bose-Fermi mixed gases of trapped atoms, in *Frontiers of Collective Motions* (World Scientific, Aizu, Japan, 2003), pp. 124–129.

[34] T. Sogo, T. Miyakawa, T. Suzuki, and H. Yabu, Random-phase approximation study of collective excitations in the Bose-Fermi mixed condensate of alkali-metal gases, Phys. Rev. A **66**, 013618 (2002).

[35] Y. Guo and H. Tajima, Medium-induced bosonic clusters in a Bose-Fermi mixture: Toward simulating cluster formations in neutron-rich matter, Phys. Rev. A **109**, 013319 (2024).

[36] H. Tajima, H. Moriya, W. Horiuchi, E. Nakano, and K. Iida, Intersections of ultracold atomic polarons and nuclear clusters: How is a chart of nuclides modified in dilute neutron matter? AAPPS Bull. **34**, 9 (2024).

[37] I. Ferrier-Barbut, M. Delehaye, S. Laurent, A. T. Grier, M. Pierce, B. S. Rem, F. Chevy, and C. Salomon, A mixture of Bose and Fermi superfluids, Science **345**, 1035 (2014).

[38] S. Falke, H. Knöckel, J. Friebe, M. Riedmann, E. Tiemann, and C. Lisdat, Potassium ground-state scattering parameters and Born-Oppenheimer potentials from molecular spectroscopy, Phys. Rev. A **78**, 012503 (2008).

[39] M. K. Tey, S. Stellmer, R. Grimm, and F. Schreck, Double-degenerate Bose-Fermi mixture of strontium, Phys. Rev. A **82**, 011608(R) (2010).

[40] M. Lu, N. Q. Burdick, and B. L. Lev, Quantum degenerate dipolar Fermi gas, Phys. Rev. Lett. **108**, 215301 (2012).

[41] T. Fukuhara, S. Sugawa, Y. Takasu, and Y. Takahashi, All-optical formation of quantum degenerate mixtures, Phys. Rev. A **79**, 021601(R) (2009).

[42] S. Sugawa, K. Inaba, S. Taie, R. Yamazaki, M. Yamashita, and Y. Takahashi, Interaction and filling-induced quantum phases of dual Mott insulators of bosons and fermions, Nat. Phys. **7**, 642 (2011).

[43] A. Salam and J. Strathdee, On goldstone fermions, Phys. Lett. B **49**, 465 (1974).

[44] E. Witten, Dynamical breaking of supersymmetry, Nucl. Phys. B **188**, 513 (1981).

[45] J. Wess and J. Bagger, *Supersymmetry and Supergravity* (Princeton University Press, Princeton, NJ, 1992).

[46] Y. Nambu and G. Jona-Lasinio, Dynamical model of elementary particles based on an analogy with superconductivity. II, Phys. Rev. **124**, 246 (1961).

[47] J. Goldstone, Field theories with superconductor solutions, Nuovo Cimento **19**, 154 (1961).

[48] S. Hoinka, P. Dyke, M. G. Lingham, J. J. Kinnunen, G. M. Bruun, and C. J. Vale, Goldstone mode and pair-breaking excitations in atomic Fermi superfluids, Nat. Phys. **13**, 943 (2017).

[49] A. V. Chumak, V. I. Vasyuchka, A. A. Serga, and B. Hillebrands, Magnon spintronics, Nat. Phys. **11**, 453 (2015).

[50] T. Zhang, D. Oue, H. Tajima, M. Matsuo, and H. Liang, Spin transport between polarized Fermi gases near the ferromagnetic phase transition, Phys. Rev. B **108**, 155303 (2023).

[51] T. Zhang, H. Tajima, and H. Liang, Magnonic spin-current shot noise in an itinerant Fermi gas, Phys. Rev. Appl. **21**, L031001 (2024).

[52] M. Sandri, A. Minguzzi, and F. Toigo, Dynamical spin-flip susceptibility for a strongly interacting ultracold Fermi gas, Europhys. Lett. **96**, 66004 (2011).

[53] J. Schwinger, Brownian motion of a quantum oscillator, J. Math. Phys. **2**, 407 (1961).
[54] L. V. Keldysh, Diagram technique for nonequilibrium processes, Zh. Eksp. Teor. Fiz. **47**, 1515 (1964).
[55] H. Tajima, D. Oue, and M. Matsuo, Multiparticle tunneling transport at strongly correlated interfaces, Phys. Rev. A **106**, 033310 (2022).
[56] A. Bilal, Introduction to supersymmetry, arXiv:hep-th/0101055.
[57] H. Tajima, D. Oue, M. Matsuo, and T. Kato, Nonequilibrium noise as a probe of pair-tunneling transport in the BCS-BEC crossover, PNAS Nexus **2**, pgad045 (2023).
[58] Y. Sekino, H. Tajima, and S. Uchino, Mesoscopic spin transport between strongly interacting Fermi gases, Phys. Rev. Res. **2**, 023152 (2020).
[59] P. Massignan, M. Zaccanti, and G. M. Bruun, Polarons, dressed molecules and itinerant ferromagnetism in ultracold Fermi gases, Rep. Prog. Phys. **77**, 034401 (2014).
[60] Y. Ji, G. L. Schumacher, G. G. T. Assumpçao, J. Chen, J. T. Mäkinen, F. J. Vivanco, and N. Navon, Stability of the repulsive Fermi gas with contact interactions, Phys. Rev. Lett. **129**, 203402 (2022).
[61] A. Amico, F. Scazza, G. Valtolina, P. E. S. Tavares, W. Ketterle, M. Inguscio, G. Roati, and M. Zaccanti, Time-resolved observation of competing attractive and repulsive short-range correlations in strongly interacting Fermi gases, Phys. Rev. Lett. **121**, 253602 (2018).
[62] J. O. Andersen, Theory of the weakly interacting Bose gas, Rev. Mod. Phys. **76**, 599 (2004).
[63] C. J. Pethick and H. Smith, *Bose–Einstein Condensation in Dilute Gases* (Cambridge University Press, Cambridge, 2008).
[64] H. Shi and A. Griffin, Finite-temperature excitations in a dilute Bose-condensed gas, Phys. Rep. **304**, 1 (1998).
[65] Z. Z. Yan, Y. Ni, A. Chuang, P. E. Dolgirev, K. Seetharam, E. Demler, C. Robens, and M. Zwierlein, Collective flow of fermionic impurities immersed in a Bose–Einstein condensate, Nat. Phys. (2024), doi:10.1038/s41567-024-02541-w.
[66] L. Viverit, C. J. Pethick, and H. Smith, Zero-temperature phase diagram of binary boson-fermion mixtures, Phys. Rev. A **61**, 053605 (2000).
[67] L. Viverit and S. Giorgini, Ground-state properties of a dilute Bose-Fermi mixture, Phys. Rev. A **66**, 063604 (2002).
[68] R. S. Lous, I. Fritsche, M. Jag, F. Lehmann, E. Kirilov, B. Huang, and R. Grimm, Probing the interface of a phase-separated state in a repulsive Bose-Fermi mixture, Phys. Rev. Lett. **120**, 243403 (2018).
[69] K. Patel, G. Cai, H. Ando, and C. Chin, Sound propagation in a Bose-Fermi mixture: From weak to strong interactions, Phys. Rev. Lett. **131**, 083003 (2023).
[70] X. Shen, N. Davidson, G. M. Bruun, M. Sun, and Z. Wu, Strongly interacting Bose-Fermi mixtures: Mediated interaction, phase diagram, and sound propagation, Phys. Rev. Lett. **132**, 033401 (2024).
[71] E. C. Stoner, Collective electron ferromagnetism, Proc. R. Soc. London, Ser. A **165**, 372 (1938).
[72] G.-B. Jo, Y.-R. Lee, J.-H. Choi, C. A. Christensen, T. H. Kim, J. H. Thywissen, D. E. Pritchard, and W. Ketterle, Itinerant ferromagnetism in a Fermi gas of ultracold atoms, Science **325**, 1521 (2009).
[73] X. Jehl, M. Sanquer, R. Calemczuk, and D. Mailly, Detection of doubled shot noise in short normal-metal/superconductor junctions, Nature (London) **405**, 50 (2000).
[74] A. A. Kozhevnikov, R. J. Schoelkopf, and D. E. Prober, Observation of photon-assisted noise in a diffusive normal metal–superconductor junction, Phys. Rev. Lett. **84**, 3398 (2000).
[75] C. D'Errico, M. Zaccanti, M. Fattori, G. Roati, M. Inguscio, G. Modugno, and A. Simoni, Feshbach resonances in ultracold $^{39}$K, New J. Phys. **9**, 223 (2007).
[76] S. E. Pollack, D. Dries, M. Junker, Y. P. Chen, T. A. Corcovilos, and R. G. Hulet, Extreme tunability of interactions in a $^{7}$Li Bose-Einstein condensate, Phys. Rev. Lett. **102**, 090402 (2009).
[77] T. Kishimoto, J. Kobayashi, K. Noda, K. Aikawa, M. Ueda, and S. Inouye, Direct evaporative cooling of $^{41}$K into a Bose-Einstein condensate, Phys. Rev. A **79**, 031602(R) (2009).
[78] S. Tan, Energetics of a strongly correlated Fermi gas, Ann. Phys. (NY) **323**, 2952 (2008).
[79] S. Tan, Large momentum part of a strongly correlated Fermi gas, Ann. Phys. (NY) **323**, 2971 (2008).
[80] S. Tan, Generalized virial theorem and pressure relation for a strongly correlated Fermi gas, Ann. Phys. (NY) **323**, 2987 (2008).
[81] N. Sannomiya and H. Katsura, Supersymmetry breaking and Nambu-Goldstone fermions in interacting Majorana chains, Phys. Rev. D **99**, 045002 (2019).
[82] P. Marra, D. Inotani, and M. Nitta, 1D Majorana goldstinos and partial supersymmetry breaking in quantum wires, Commun. Phys. **5**, 149 (2022).
[83] U. Miura and K. Totsuka, Supersymmetry breaking in a generalized Nicolai model with fermion pairing, arXiv:2308.03346.